1996ApJ...465..264P

THE ASTROPHYSICAL JOURNAL, 465:264–277, 1996 July 1
© 1996. The American Astronomical Society. All rights reserved. Printed in U.S.A.

ASTROMETRIC DETECTION OF EXTRASOLAR PLANETS: RESULTS OF A FEASIBILITY STUDY WITH THE PALOMAR 5 METER TELESCOPE[1, 2]

STEVEN H. PRAVDO
Jet Propulsion Laboratory, Mail Stop 306-438, California Institute of Technoloty, Pasadena, CA 91109; spravdo@ccmail.jpl.nasa.gov

AND

STUART B. SHAKLAN
Jet Propulsion Laboratory, Mail Stop 306-388, California Institute of Technology, Pasadena, CA 91109; shaklan@huey.jpl.nasa.gov
Received 1995 July 17; accepted 1996 January 10

ABSTRACT

The detection of extrasolar planets around stars like the Sun remains an important goal of astronomy. We present results from Palomar 5 m observations of the open cluster NGC 2420 in which we measure some of the sources of noise that will be present in an astrometric search for extrasolar planets. This is the first time that such a large aperture has been used for high-precision astrometry. We find that the atmospheric noise is 150 μas hr$^{1/2}$ (1 μas = 1 micro-arcsecond) across a 90″ field of view and that differential chromatic refraction (DCR) can be calibrated to 128 μas for observations within 1 hr of the meridian and 45° of zenith. These results confirm that a model for astrometric measurements can be extrapolated to large apertures.

We demonstrate, based upon these results. that a large telescope achieves the sensitivity required to perform a statistically significant search for extra solar planets. We describe an astrometric technique to detect planets, the astrometric signals expected, the role of reference stars, and the sources of measurement noise: photometric noise, atmospheric motion between stars, sky background, intrumental noise, and DCR. For the latter, we discuss a method to reduce the noise further to 66 μas for observations within 1 hr of the meridian and 45° of zenith. We discuss optimal lists of target stars taken from the latest Gliese & Jahreiss catalog of nearby stars with the largest potential astrometric signals, declination limits for both telescope accessibility and reduced DCR, and galactic latitude limits for a sufficiant number of reference stars. Two samples are described from which one can perform statistically significant searches for gas giant planets around nearby stars. One sample contains 100 "solar class" stars with an average stellar mass of 0.82 $M_\odot$; the other maximizes the number of stars, 574, by searching mainly low-mass M stars. We perform Monte Carlo simulations of the statistical significance of the expected results by using measured and estimated noise quantities. We show the semimajor axis parameter spaces that are searched for each star and how an increase in the length of the observing program expands these spaces. The search over semimajor axis parameter space relates to the theory of gas giant planet formation.

Subject headings: astrometry — atmospheric effects — methods: data analysis — open clusters and associations: individual (NGC 2420) — planetary systems

1. INTRODUCTION

1.1. *Background*

The question "Do other stars have planets?" is of interest to scientists and nonscientists alike. Recently, Mayor & Queloz (1995), using radial velocity observations, reported the discovery of the first extrasolar planet orbiting a solar-like star. The star is 51 Pegasi, and the planet is in a 4 day orbit (see also Marcy & Butler 1995). The lower limit to the 51 Peg companion mass is 0.5 Jupiter masses (M_J), while Mayor & Queloz estimate the upper limit to be $2M_J$ based upon their inference of the system inclination angle. Pravdo et al. (1995a) argue that the 51 Peg companion is a planet independent of knowledge of the system inclination angle because of the solar-like X-ray emission from the system.

Radial velocity programs (e.g., Latham et al. 1989; Marcy et al. 1993; McMillan et al. 1994) continue to search for planets but are hindered by the uncertainty in the companion masses due to the unknown system inclination angles (e.g., Cochran, Hatzes, & Hancock 1991). Other inferred planet detections using infrared spectroscopy (Marsh & Mahoney 1992, 1993) are subject to alternative interpretations (Boss & Yorke 1993). The detection of planets around a pulsar (Wolszczan & Frail 1992) is on firmer ground (but see Gil et al. 1993; Peale 1993) but may be unrelated to the solar-like planetary systems that we consider herein.

Astronomy is another technique used in planet detection programs (e.g., Gatewood 1987). We discuss herein recent astrometric results and the application of these results to planetary detection. Astrometry is complementary to radial velocity measurements, since systems with large astrometric signals (§ 6) tend to have small radial velocities. Furthermore, astrometric results are insensitive to the system inclination angle.

Both theoretical models and observational evidence lead us to conclude that the solar system is not the result of an improbable path of stellar evolution and therefore, that planetary systems are common. Black & Matthews (1985) and Levy et al. (1992) have compiled much of the theory and observational evidence on solar system formation. The

[1] The research described in this paper was carried out in part by the Jet Propulsion Laboratory, California Institute of Technology, under contract with the National Aeronautics and Space Administration.

[2] Based in part on observations made at Palomar Observatory, California Institute of Technology.

© American Astronomical Society • Provided by the NASA Astrophysics Data System

1996ApJ...465..264P

observations describe an evolutionary chain from protostars, through pre–main-sequence stars, to stars like the Sun. Circumstellar disks (e.g., Smith & Terrile 1984) are a common phenomenon in young stars and may be the precursors of planetary systems.

The solar system is believed to have formed from a protosolar nebula (e.g., Safronov 1969). The planets are organized into two types: gas giants (Jupiter, Saturn, Uranus, Neptune) and terrestrial planets (Earth, Mars, Venus, Mercury). Gas giants form beyond the water condensation radius, a distance from the center of the nebula beyond which water and other abundant volatiles remain solid (e.g., Safronov & Ruskol 1994), while terrestrial planets form within this radius. Pluto is an anomaly. Gas giants are also 10–300 times more massive than terrestrial planets because more planet-forming material is available at their locations. Based on the solar model, the astrometric search for gas giants is easier than for terrestrial planets because they are more massive and further from the star, both contributors to larger astrometric signals.

1.2. *Extrasolar Planet Detection*

Extrasolar planet detection is a unique task because the best targets are well known and unlikely to change. Other than unidentified, low-mass M stars, most of the stars within 25 pc of the Sun are known. It remains only to implement a detection technique within a systematic program to find planets assuming they exist. The search for planetary systems is contributing to the development of many new intruments and techniques designed to solve the difficult problem of planet detection (Burke et al. 1993).

The astrometric signals from putative planetary systems are well defined. They depend on the planet-star mass ratio, the planet-star separation, and the distance to the star. The sources of noise are many. In the visible, using a ground-based single-aperture telescope and an area detector, they include photon noise, atmospheric noise, sky background noise, uncalibrated differential chromatic refraction (DCR), detector noise, uncalibrated geometric errors on the detector, and uncalibrated optical aberrations. We have undertaken a program to measure the sources of noise which cannot be modeled reliably. For example, Shaklan et al. (1995) demonstrate a method to calibrate geometric errors on CCD pixels to a level of 0.01 pixels. Herein we present results from Palomar 5 m observations that are relevent for atmospheric noise and DCR.

Atmospheric noise may be the limiting factor for high-precision ground-based astrometry. Lindegren (1980) shows that the astrometric motion between two stars separated by an angle θ due to the atmosphere is proportional to θ^{-1} in the narrow-angle regime: for large apertures the narrow-angle regime extends to several arcminutes. The motion also varies with aperture diameter as $D^{-2/3}$ (Shao & Colavita 1992). Observations of star pairs confirm this behavior (Gatewood 1991; Colavita 1994; Dekany et al. 1994).

Our measurements, discussed below, are for a field of 15 stars within 90″. Lindegren (1980) also addresses the case of a field of stars and gives equations (his eqs. [29] and [36]) for the limiting case of a target star centered among an infinite number of reference stars in a finite field. We have expanded Lindegren's treatment for a finite reference star distribution (§ 5 and Appendix A) and present an analysis which shows that our results match the theoretical prediction, demonstrating the efficacy of the large aperture.

This paper is organized in the following way. First, we present Palomar 5 m observations of the open cluster NGC 2420 and discuss our results. Then we describe the astrometric technique for planet detection and present new estimates of the measurement noise based upon our 5 m results. Finally, we describe the implications of our results with particular emphasis on the ability to make a statistically significant survey of nearby stars for planets using a large-diameter ground-based telescope.

2. OBSERVATIONS

We observed the open cluster NGC 2420 on 1995 February 5 at the F/16 Cassegrain focus of the Palomar 5 m (200 inch) telescope using the CCD-13 camera. CCD-13 is a SITe 2048 × 2048 backside-illuminated device with 24 μm square pixels. The camera is attached to the f/9 base and guider assembly (McCarthy 1994). The f/9 optics were not used.

NGC 2420 is a high galactic latitude cluster that was chosen because of its position, passing within 9° of zenith and transiting at 0^h local time. It contains a sufficient density of bright stars to permit an astrometric study that is atmospherically, rather than photometrically, limited. Detailed photometric analysis of this cluster has been carried out by Anthony-Twarog et al. (1990). Table 1 identifies the stars used in our analysis, their magnitude, and color using Table 2 of Anthony-Twarog et al. The identification numbers are from West (1967). Figure 1 is a plot of the positions of the stars with their West identifications.

The pixes size on the CCD is 24 μm, resulting in a pixel scale of 61 milliarcsec (mas) pixel^{-1} and a field of view (FOV) 124″ wide. The CCD was oriented with R.A. increasing along columns and declination decreasing along rows. The CCD showed no evidence of bad columns, but the lower left portion of the field was obscured by the guide camera periscope, which had frozen in place early in the evening. Stars that may have been partially vignetted by the periscope were not used in this study. The CCD read noise was 6.7 e^-, and its gain was set to 1.8 e^- per data number.

The cluster was observed from 19 minutes east to 3 hr west of meridian. A set of 55 1 minute exposures was made at ~3.3 minute intervals. The position of the cluster on the CCD was not moved during the first 24 exposures. During the 25th exposure, a pointing error caused by slippage of

TABLE 1

STARS OBSERVED IN NGC 2420

Identification (1)	x (2)	y (3)	V (4)	B-V (5)	$R_{\rm eff}$ (6)
1116.....	46″	19″.4	13.68	−0.003	16.24
2108.....	33.5	17.1	14.48	0.433	−0.49
2111.....	19.1	18.7	14.27	0.433	−0.45
2116.....	9.5	16.1	14.57	0.419	0.62
2119.....	−3.2	5.7	14.56	0.424	0.54
2120.....	0	0	14.5	0.417	1.57
2114.....	17.1	3.4	14.28	0.469	−0.77
2127.....	8.8	−11.4	14.51	0.432	0.55
2128.....	14.6	−15.7	15.37	0.502	−1.5
2129.....	19.2	−16.1	15.65	0.534	−2.52
2122.....	−24.1	1.1	14.49	0.866	−11.7
2225.....	−32.5	−4.7	15.98	0.485	−1.58
2226.....	−41.3	−8.6	15.05	0.445	−0.39
2227a	−36.3	−16.4	14.62	0.41	0.43
J.....	−45.5	24.9	13.95	0.433	−0.54

© American Astronomical Society • Provided by the NASA Astrophysics Data System

1996ApJ...465..264P

TABLE 2

ROOT MEAN SQUARE PHOTOMETRIC BIAS AND FRAME-TO-FRAME CENTROID NOISE

	1 MINUTE EXPOSURES			10 MINUTE INTEGRATIONS	
STAR (1)	Photon Noise (2)	R.A. Noise (3)	Decl. Noise (4)	R.A. Noise (5)	Decl. Noise (6)
1116	0.19	1.25	2.05	0.12	0.37
2108	0.24	0.52	0.86	0.18	0.59
2111	0.25	0.42	0.75	0.05	0.29
2116	0.30	0.60	1.16	0.08	0.43
2119	0.26	0.55	1.19	0.35	0.32
2120	0.24	0.77	1.10	0.25	0.32
2114	0.22	0.49	0.65	0.13	0.95
2127	0.29	0.57	0.89	0.06	0.23
2128	0.51	0.72	1.47	0.40	0.30
2129	0.62	0.56	2.81	0.33	0.66
2122	0.23	0.52	0.76	0.07	0.10
2225	0.86	1.58	1.50	0.19	0.27
2226	0.40	1.12	1.49	0.40	0.41
2227a.....	0.30	0.94	1.40	0.31	0.36
J	0.20	0.70	1.09	0.16	0.35

NOTE.—All values are in units of mas (rms).

the guider periscope resulted in a 5″ shift of frames 26–55 compared to 1–24. As explained below, the two sets cannot be compared accurately at the 0.1 mas level. Thus, we analyze the data in two sets, A and B, representing frames 1–24 and 26–55, respectively.

Atmospheric conditions were excellent and at times yielded sub-arcsecond seeing. During the observations the outside temperature decreased by 0.2°C while the dome air, which was nominally 2°C cooler, warmed by 0.1°C. The observations were made on the second night of a stable 3 day weather pattern. The sky was clear except for cirrus near the west horizon.

The astrometric observations were made using a bandpass color filter composed of a long-pass and short-pass filter placed in series in the filter wheel of the f/9 base. The filters were manufactured by CVI Laser Corp. on plate glass. The long-pass filter has a cut-on wavelength of 550 nm, with attenuation >99% below 525 nm and full transmission at 575 nm. The short-pass has a cutoff at 750 nm, with full transmission to 740 nm and attenuation >99% beyond 775 nm. Because they are built on plate glass, local gradients in the wave fronts passing through the filters result in positional errors >1 mas. This is why our experiments required that the stars remain stationary to ~1″ during the observations. The 5″ guiding error in frame 25 caused one star to be displaced by 6 mas relative to the other stars. Future astrometric programs will require accurately calibrated, flatter filters.

We also observed the cluster through three bandpass filters. These were centered at 550, 650, and 750 nm, each with full width at half-maximum (FWHW) of 40 nm. The purpose of these observations was to calibrate the differential chromatic refraction in the frame. This will be explained further below.

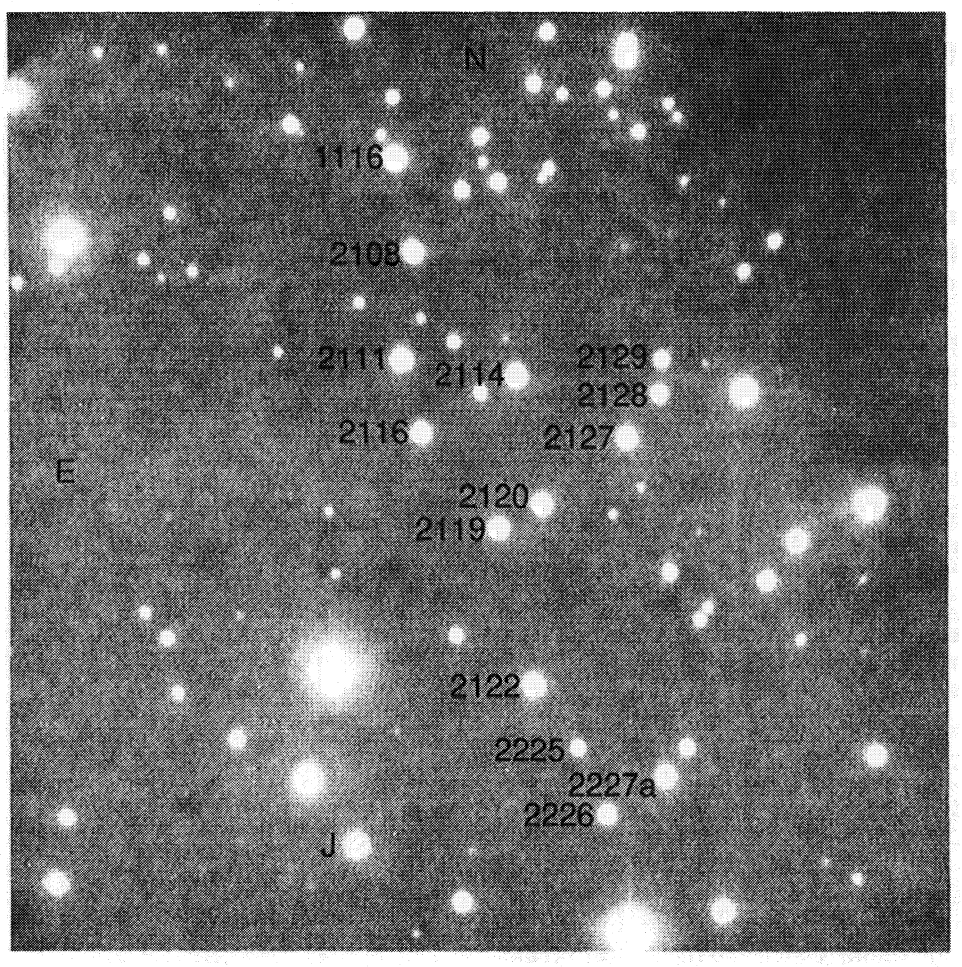

FIG. 1.—These stars in NGC 2420 were observed with the Palomar 5 m telescope

© American Astronomical Society • Provided by the NASA Astrophysics Data System

1996ApJ...465..264P

3. DATA REDUCTION

The astrometric reduction of the frames followed four steps: centroiding, removal of differential chromatic refraction (DCR), fitting with a plate scale model, and computation of the Allan variance for each star. DCR is removed from the data before the data is fitted with a linear model. However, as described below, residual DCR (due to poor calibration) is observed.

3.1. *Centroiding*

Centroids were computed by centering a 4″.9 × 4″.9 (80 × 80 pixel) box on each of the 15 stars. Two types of centroids were computed with the box: the first moment of the marginal distribution, and a Gaussian fit to the image. The moment was chosen because of its simplicity and insensitivity to aberrations. The Gaussian was chosen because its performance has been shown to be competitive with several more complicated alogrithms as demonstrated by Stone (1989).

The moment was computed (for the row direction) using

$$x_c = \frac{\sum I_{ij} \times i - B}{\sum I_{ij} - B} . \quad (1)$$

The background B was determined for each frame by averaging two 6″ × 6″ regions without detectable stars on the CCD. Unlike Stone (1989), images were not trimmed to increase centroiding precision for fear of loss of accuracy.

An elliptical Gaussian function was also fitted to the images. Parameters of the fit were the amplitude, x and y center, position angle of the major axis, major and minor axial widths, and background level. The procedure used was to fit all seven parameters to star 1116, then to fix the shape parameters, fitting only amplitude, x and y center, and background on the remaining stars.

In practice we found that the first moment performed as well on average as the Gaussians. Each resulted in a frame-to-frame standard deviation of ~1 mas. This is consistent with the observed centroid noise being largely due to atmospheric statistics rather than photon and background statistics. The first moment variances still show dependence on source brightness, while the Gaussian performance appears to be limited by systematic effects. This is due in large part to the mismatch between the symmetrical Gaussians and the slightly asymmetrical, aberrated images. The mismatch led to a 10% fitting error at the image peak, and a poor estimate of the image wings. For observations of background-limited sources, an improvement on the Gaussian fits would be required. But for the purposes of this analysis, in which the centroid noise is largely dominated by the atmosphere, the simple first moment approach is adequate. In what follows, only the centroids obtained by the first moment calculations are discussed.

3.2. *Correction of Differential Chromatic Refraction (DCR)*

DCR results in relative astrometric errors (e.g., Monet et al. 1992). As stars move away from the meridian, the bluer stars in the frame appear to shift toward the zenith, while the red stars appear to shift toward the horizon. We calibrate DCR for our reference fields in the following way. We observe broad band in the visible avoiding water absorption bands in the near-infrared. Then we estimate the blackbody temperatures of the target and reference stars in the field by observing them with the three bandpass filters. Note that these filters fall within the astrometric filter band.

DCR is quadratic in wavenumber. A fit to the data in Allen (1973) for λ = 500–800 nm yields the refractive constant $R(\lambda)$ for an air temperature of 0°C and pressure of 760 mm Hg:

$$R(\lambda) = 59.24 + \frac{346466}{\lambda^2} \text{ arcsec} , \quad (2)$$

where the wavelength is expressed in units of nm. The refractive constant changes by hundreds of milliarcseconds across the visible and near-IR spectrum. Thus, it is critical to characterize accurately the refractive constant of the stars to remove color-dependent centroid shifts. The temperature dependence of $R(\lambda)$ is ~40% for a 10° change.

The effective refractive constant for a star, $R_{\rm eff}$, depends on the spectrum of the star, $I(\lambda)$, the bandpass set by the filter, $T(\lambda)$, and the CCD quantum efficiency, $Q(\lambda)$. The refractive constant is given by the normalized product of these quantities:

$$R_{\rm eff} = \frac{\int R(\lambda)T(\lambda)Q(\lambda)I(\lambda)d\lambda}{\int T(\lambda)Q(\lambda)I(\lambda)d\lambda} . \quad (3)$$

$Q(\lambda)$ is obtained from the calibrated CCD-13 response. $T(\lambda)$ is between 550–750 nm and is described quantitatively by the filter specifications. The total refraction observed is given to first order by $R_{\rm eff}$ tan (z), where z is the apparent zenith angle.

We do not know $I(\lambda)$ independently for many of the program stars. Instead, we use an approximation for $I(\lambda)$ determined for each star from its intensities measured through the three narrow bandpass filter. These data are divided by the filter tranmission functions and CCD quantum efficiency and fitted to blackbody curves. The only parameter of this fit is the blackbody temperature. Once fitted, the blackbodies are used as $I(\lambda)$ in equation (3) to determine $R_{\rm eff}$.

We used standard spectra of several dozen stars of all spectral types (Jacoby et al. 1984) to estimate the effectiveness of this technique. The above procedure was applied to the stellar spectra, and the refractive constant derived from the blackbody fit was compared to that obtained for the stellar spectrum. For dwarf stars ranging in spectral type from B4 to M5, the estimated refractive constant had a standard deviation of 0.43 mas when comparing the true and modeled $I(\lambda)$.

For the NGC 2420 observation, the narrow bandpass filter transmissions were calibrated using standard stars with an accuracy of 2%. This is not a critical measurement because all stars in the cluster are observed simultaneously through the same filter. Filter calibration errors then have a negligible effect on the relative blackbody temperature estimates and thus the relative DCR of all stars in the field of view.

Once the refractive constants are determined, the estimated DCR centroid shifts are removed from the measured centroid positions. As the temperature was constant to 0.2°C during the observations, no thermal corrections were applied to the estimated DCR terms. We emphasize that since only relative astrometry within a frame is performed, the temperature dependence of the calibration depends only on the second term of equation (2). For example, given a star with a refractive constant of 10 mas relative to the other

© American Astronomical Society • Provided by the NASA Astrophysics Data System

1996ApJ...465..264P

stars in the frame, a 10°C change during the observations leads to 0.4 mas error in its position. A more detailed description of the temperature and pressure dependence of the DCR correction is given by Monet et al. (1992).

3.3. *Plate Scale Model*

The corrected centroids were next fitted frame by frame to a linear plate scale model with six linear constants defined by

$$x(i, r) = a_f x(i, f) + b_f y(i, f) + c_f \quad (4)$$

$$y(i, r) = d_f x(i, f) + e_f y(i, f) + g_f \,. \quad (5)$$

A reference frame r was chosen, so that each star i in frame f was fitted to star i in frame r using a least-squares solution in which all stars received equal weight.

We defined a target star and reference frame by excluding each star in turn from the model, which was then fitted to the remaining 14 stars. To evaluate the effect of turbulence without removing frame-to-frame plate-scale variation, we performed a second data reduction in which the plate scale constants a, b, d, and e were first fitted by a quadratic function of the form $a = a_o + a_q t^2$, where t is the time of observation. This provided correction for gradual telescope defocus and sag, as well as differential atmospheric refraction (nonchromatic) between azimuth and elevation.

3.4. *Allan Variance*

The astrometric program discussed in the later sections of this paper relies on a $\sqrt{t}$ improvement in astrometric precision to achieve the sensitivity required to detect extrasolar planets. Atmospheric models predict that differential astrometric measurements exhibit a white power spectrum and therefore improve as $\sqrt{t}$ for interframe $t \gtrsim 1$ s (Colavita 1994). We compute the Allan (1966) variance for the atmospheric noise to characterise the improvement in astrometric precision versus integration time. The calculation also indicates the level of systematic errors in the data. The Allan variance for the combined atmospheric and photometric noise is given by (Colavita 1994):

$$\sigma_x^2 = \frac{1}{2(M+1-2l)} \sum_{n=0}^{M-2l} \left(\frac{1}{l} \sum_{m=1}^{l-1} x_{n+m} - x_{l+n+m} \right)^2 , \quad (6)$$

where M is the total number of frames, l is the lag, and x is the measured stellar position. The atmospheric noise is derived from $\sigma_a^2 = (\sigma_x^2 - \sigma_p^2)^{1/2}$, where σ_p is the positional error due to photometric noise. For $\sqrt{t}$ behavior, the Allan variance has a slope of -1 on a log-log plot of centroid motion versus integration time. The slope flattens and can eventually reverse itself when systematic errors become significant with respect to the noise in time-integrated data.

4. RESULTS

After computing the first-moment centroids for each star, the positions were corrected for DCR. The refractive constant $R_{\rm eff}$ was determined using the three-filter method described above, then multiplied by tan (z) and subtracted from the measured centroids. Column (6) of Table 1 gives $R_{\rm eff}$ for each of the 15 stars. For the frames in set B, tan (z) ranged from 0.38 to 0.90, yielding refractive corrections that changed by 8.4 mas for star 1116 and -6.08 mas for star 2122. The accuracy of the corrections is estimated to be 0.43 mas at tan (z) = 1(§ 3.2).

The corrected positions were then fitted using the linear plate scale model. The model shows a significant discontinuity between data sets A and B of $\sim$4 mas. The discontinuity is not related to either CCD or telescope distortion. While CCD step-and-repeat errors of 0.5 μm have been measured on another CCD (Shaklan et al. 1995), those errors were accompanied by flat-field patterns indicative of the step-and-repeat geometry. These patterns are not seen in the Palomar CCD-13, so it does not have large pixel-scale errors. Another potential source of distortion is the telescope optics. Models of the Palomar 5 m show that for alignment tolerances of 1′ and 1 mm in secondary mirror tilt and displacement, respectively, telescope distortion remains below 0.2 mas across a 2′ field of view. The most likely source of displacement between data sets A and B is the poor quality of the bandpass filter. The filter is built on float glass and has wave front gradients of several waves per millimeter in various orientations.

After applying the plate scale model, the star trails should exhibit random noise that is uncorrelated with zenith angle. Errors in the DCR calibration lead to correlation which is measured by fitting the residual star positions and tan (z). We find that for the 15 stars, the standard deviation of the fitting coefficient is 1.31 mas, some of which is systematic drift due to DCR calibration effects. To investigate the DCR contribution, we ran a Monte Carlo simulation of centroid data with the same geometry as the observed stars. Star centroids were sampled from a Gaussian distribution having a standard deviation of 0.96 mas in R.A. and 1.5 mas in declination, as seen in the real data. Thirty-one frames were generated to simulate data set B. These were fitted with a linear plate scale model, then the residual star positions were fitted to tan (z). The standard deviation of the fitting coefficient was found to be 1.17 mas. Thus, most of the 1.31 mas of correlation in the real data was due to the random statistics of the frame and is not attributable to DCR calibration errors. The part that is attributable to DCR errors is $(1.31^2 - 1.17^2)^{1/2} = 0.59$ mas. This is close to the predicted error of 0.43 mas detailed above. In data set B, tan (z) spanned 0.38–0.90. For this range, the standard deviation of centroid positions due to DCR calibration errors was $0.59(0.9 - 0.38) = 0.31$ mas.

The Allan variance was computed for each star. The variances are biased by photometric noise due to photon statistics, read noise, and sky background. We estimated the photometric noise bias by employing a Monte Carlo simulation; first we took an image of a star from one of the frames, then added background noise, read noise, and photon noise according to the flux of each star. Background and read noise were estimated by comparing pixels in several frames from a starless region of the frame. Then we computed the first moment and repeated the Monte Carlo procedure 100 times for each star. The root mean squared (rms) photometric bias and de-biased frame-to-frame centroid rms are given in Table 2.

The square root of the de-biased Allan variance for the the 15 stars is plotted in Figure 2. These curves are for data set B, containing 31 1 minute exposures. The frames cover hour angles $1^{\rm h}14^{\rm m}$ to $3^{\rm h}3^{\rm m}$. Each curve represents the improvement in astrometric precision of one star. The two dashed lines indicate $\sqrt{t}$ behavior. The values at the left edge of the plots can be found in columns three and four of Table 2. The root sum squared (rss) noise for all 1 minute exposures is 0.82 mas in R.A. and 1.39 mas in declination. When grouped into 10 minute integrations, the rss value is 0.23 mas in R.A., 0.37 mas declination. This result, when

© American Astronomical Society • Provided by the NASA Astrophysics Data System

1996ApJ...465..264P

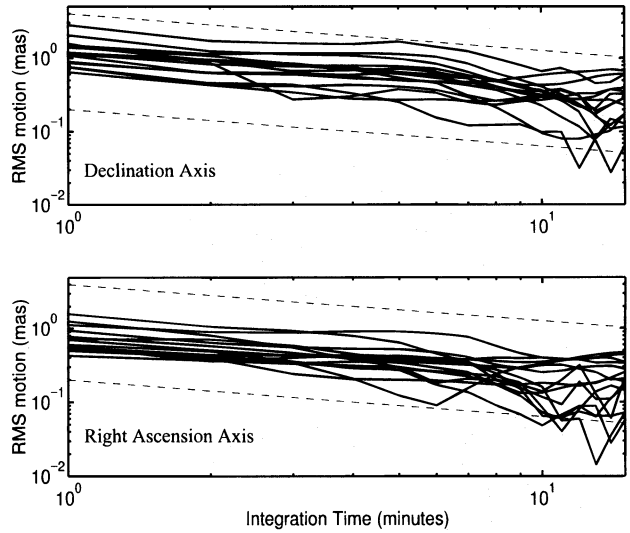

FIG. 2.—The square root of the Allan variance of the positional uncertainty of 15 stars in NGC 2420 observed with the Palomar 5 m. *Top*: Declination. *Bottom*: Right ascension.

extrapolated to a 1 hr integration and a 90″ field of view, yields 150 μas hr$^{1/2}$ noise. These numbers show that the mean astrometric precision is improving by $\sqrt{t}$ and that precisions of 0.23 mas can be achieved without systematic limitation.

The curves do not all decrease monotonically with integration time. This has been shown through Monte Carlo simulations of the observations to be consistent with the finite number of frames and stars, and it is not indicative of systematic limitations.

5. EXPERIMENTAL CONCLUSIONS

5.1. *Field Averaging*

The spread of the curves in Figure 2, and the difference between the declination and R.A. results, can be explained by the location of the stars relative to the field centroid. Stars near the center of the field have lower noise relative to the target star than stars near the edge. For astrometry of a target star relative to a reference frame of stars, the variance of the astrometric position due to atmospheric turbulence is given by (in arcsec^2)

$$\epsilon^2 = \frac{2.9 \times 10^{-5}}{n^2 t}\left[\sum_{i=1}^{n}\sum_{j=1}^{n} D^{-4/3}\left(\delta_{0i}^2 - \frac{1}{2}\delta_{ij}^2\right) - 192\sum_{i=1}^{n}\sum_{j=1}^{n} D^{-2}\left(\delta_{0i}^{8/3} - \frac{1}{2}\delta_{ij}^{8/3}\right)\right], \quad (7)$$

where the target star is represented by subscript 0, and the n reference stars are represented by subscripts i and j. Here δ_{ij} is the angular separation of stars i and j projected onto a line, expressed in radians. D is the telescope diameter in meters, and t is the integration time in seconds. This equation is based on Lindegren (1980) and is derived in Appendix A. It assumes a Kolmogorov turbulence spectrum, a Hufnagel (1994) turbulence profile, and seeing parameter of $r_0 = 10$ cm. The equation reduces to the binary star equation (Lindegren 1980) for two stars and separations greater than a few arcseconds.

The data were analyzed and compared to equation (7) using the astrometric data reduction process described in § 3.3. Scale changes due to slow focus drift were incorporated into the plate scale model. Each of the 15 stars was taken in turn to act as the target star. Figure 3 shows the astrometric precision for each star in data set B for 1 minute exposures for both the R.A. and declination axes. The x-axis of the plot is the "star number" in the same sequence as the listing in Table 1. A comparison of the list shows that the stars are ordered roughly with decreasing declination. Thus, star 1 and star 15 are the edge stars, furthest from the frame centroid.

The measured mean positions for the remaining 14 reference stars were entered into equation (7), which was evaluated to yield the dashed curves of Figure 3. The curves show that equation (7) is a good predictor of astrometric precision in a field of reference stars. The differences between R.A. and declination also show that the noise is largest in the direction of greatest field radius, and that equation (7) is able to predict this effect.

Stars 5 and 6 (2119 and 2120, respectively) are closest to the geometric center of the field (offset by 3″.5 and 2″.2 in R.A. and 2″.2 and 1″.0 in decl., respectively). Both the observations and equation (7) show that even for these small separations, the astrometric accuracy is limited to about 1 mas in 60 s of observation at the 5 m telescope. The limitation comes from the second term of equation (7); this is the same term (multiplied by a factor of 6) that appears in Lindegren's (1980) formula for the limiting case of a symmetric field with infinitesimally spaced stars.

The match between equation (7) and our data is a powerful result because it demonstrates that equation (7) can predict the astrometric precision for a random set of reference stars. One obvious application is the predetermination of the precision of an astrometric program by applying equation (7) to any known reference field. As seen in Figure 3, the precision can easily fluctuate by a factor of 2–3 (corresponding to integration time factors of 4–9) depending on the background star distribution.

5.2. *Significance*

It is useful to place our findings in the context of previous work. The vast majority of astrometric work has taken place on telescopes with apertures ≤ 1.5 m (e.g., Monet et al. 1992; Gatewood et al. 1987). The best astrometric precisions obtained in long-term programs are 0.4–1.0 mas (Stone & Dahn 1994). The limiting precision is attributed to

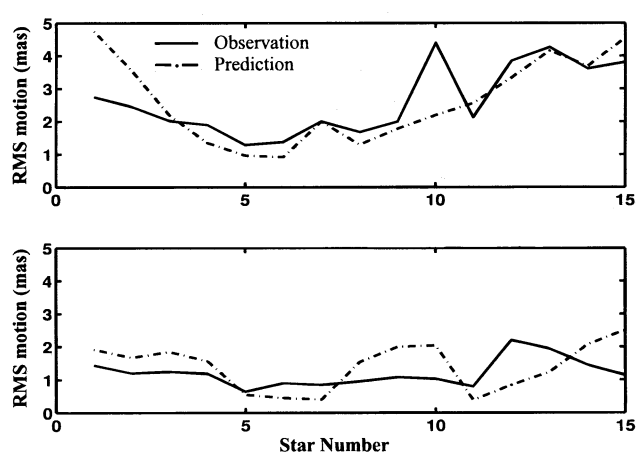

FIG. 3.—This shows the measured vs. predicted astrometric accuracies for the 15 stars observed in NGC 2420 with the Palomar 5 m. The predictions are derived from eq. (7). *Top*: Declination axis. *Bottom*: Right ascension axis. $T = 60$ s in both cases.

© American Astronomical Society • Provided by the NASA Astrophysics Data System

1996ApJ...465..264P

DCR (Monet et al. 1992). In a program with a larger aperture, the Kitt Peak National Observatory 4 m telescope, Monet & Dahn (1983) also identify DCR as the largest source of error. The DCR limitation was partly due to the wide bandpasses employed, and to the nature of their target stars which were extremely red. These limitations are not present in our results.

Despite years of observations, none of these surveys have approached the systematic limitations imposed by the CCD and optics. Our new 5 m results reach a precision of 0.1 mas and show that this precision is not limited by the CCD or optics. We demonstrate also for the first time that the extrapolation of Lindegren's theory is valid for large apertures, and that the astrometric precision of a field, known to be highly dependent on the nature of the reference frame (Stone & Dahn 1994), is predicted accurately from the distribution of reference stars relative to the target star.

These observations do not address long-term systematic errors. In the following we show how our results, along with assumptions about the long-term performance of the instrumentation and DCR calibration, lead to new conclusions about the ability to detect extrasolar planets with ground-based telescopes.

6. SOURCES OF NOISE IN PLANET DETECTION

6.1. *Planetary Signal and Noise*

In the astrometric method of planet detection, one measures the motion of the stars around their planetary system centre of mass. Consider the simplest case of a single planet orbiting a single star in a circular orbit. Then the astrometric signal Θ of the star is

$$\Theta(\mu\text{as}) = 960\left(\frac{a}{5\ \text{AU}}\right)\left(\frac{10\ \text{pc}}{d}\right)\left(\frac{M_p}{M_J}\right)\left(\frac{M_\odot}{M_S}\right), \quad (8)$$

where a is the semimajor axis of the planetary orbit, d is the distance to the star, (M_p/M_J) is the planet-to-Jupiter mass ratio, and $(M_S/M_\odot)$ is the stellar mass in solar units (Fig. 4). The period T of the planet is

$$T(\text{yr}) = 11\left(\frac{a}{5\ \text{AU}}\right)^{1.5}\left(\frac{M_\odot}{M_S}\right)^{0.5}. \quad (9)$$

Note that the orbital period is an important observational parameter since it defines the observing program length

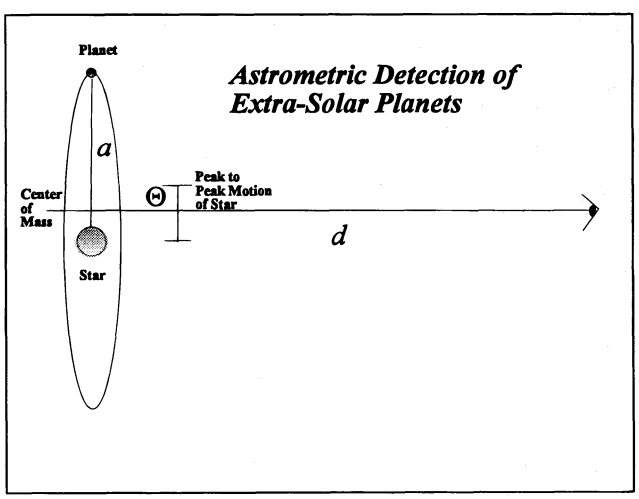

FIG. 4.—The planet-star configuration illustrates the astrometric signal produced.

and, for fixed M_S, Θ is proportional to $T^{0.67}$. Planets arising from protostellar nebulae are expected to be in circular or nearly circular orbits on both theoretical and observational grounds, but even if the orbits are noncircular, the reduction in the signal strength (i.e., the power in the main harmonic) is small (Black & Scargle 1982).

The astrometric data Σ from the target star corrected to the solar barycenter and, which we simplify from two dimensions to one, can be written

$$\Sigma(t) = \left(\frac{\Theta}{2}\right)\sin\left(2\pi\frac{t}{T} + \phi\right) + \mu t + P\sin(2\pi t) + c + \sigma_o, \quad (10)$$

where t is the time of observation, Θ is the amplitude or signal, ϕ is the orbital phase at time zero, μ is the proper motion, P is the parallax, c is the mean position, and σ_o is the standard deviation of the noise per observation. It is estimated from the data by determining the exposure-to-exposure target star motion relative to the reference stars. One can detect a planetary signal in a time sequence of such data in a number of ways including Fourier or periodogram (Black & Scargle 1982) analysis.

For what follows, we choose a CCD as the astrometric detector. The noise σ_o is the rss of atmospheric, photometric, and DCR noise, viz:

$$\sigma_o = \left[\frac{(o_a^2 + o_p^2)}{t} + o_{\text{DCR}}^2 + o_{\text{CCD}}^2 + o_{ab}^2\right]^{0.5}, \quad (11)$$

where σ_a is the atmospheric noise taken from equation (7); σ_p is the photometric noise including photon statistics, sky background, and detector noise; σ_{DCR} is the DCR; σ_{CCD} is any systematic positional error due to CCD spatial nonuniformity; σ_{ab} is the positional error due to optical aberrations; and t is the observation time. Thus, atmospheric and photometric noise decrease with time, while the rest are systematic terms.

6.2. *Detection Requirements*

A Monte Carlo program is used to determine the probability that the signal in equation (10) is real and not simply a noise artifact. First we create simulated 10 yr data sets containing nonzero values for all five parameters and noise of σ_o per measurement. The uncertainties in μ and P were taken to be 0".1 yr^{-1} and 0".1, respectively, compared to the typical values of 1" yr^{-1} and 0".1, respectively. This yields an estimate of amplitude, period, and phase for the stellar motion. Then we perform a nonexistence test on the measured amplitude by setting Θ to zero, fixing the period and phase to that obtained in the simulation, and generating new 10 yr data sets. For each data set, we obtain an estimated amplitude having a Gaussian distribution with standard deviation σ_Θ. The probability that the amplitude determined from the first simulation is due strictly to noise is given by the erf function (e.g., Press et al. 1989) evaluated at Θ/σ_Θ. Figure 5 shows the 3 σ_Θ values plotted versus T for data that consist of two observations per year for 10 yr with σ_o of 150 μas. For $T \leq 10$ yr, the values are independent of ϕ. For $T > 10$ yr, the 3 σ_Θ values correspond to observations with the worst possible ϕ; i.e., with the most linear portion of the sinusoid centered at $T/2$. Figure 5 can be interpreted in the following way: any stellar astrometric signal above the curve is a planet detection with at least 99.7% (3 σ) confidence. The figure shows the penalty for

© American Astronomical Society • Provided by the NASA Astrophysics Data System

1996ApJ...465..264P

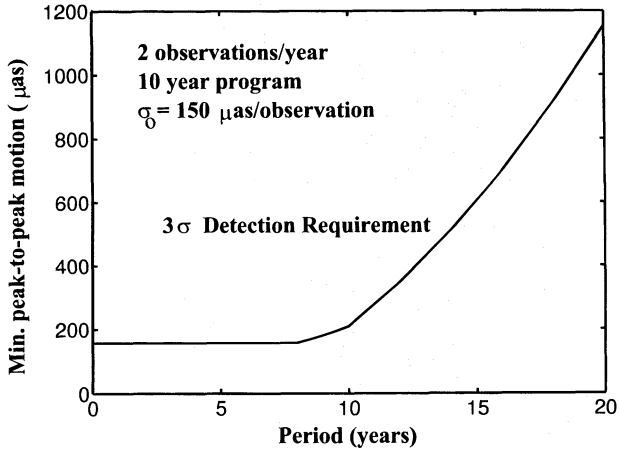

FIG. 5.—Minimum peak-to-peak amplitudes of stellar motion for 3 σ detections vs. the orbital period of a planet. The plot assumes two observations per year for 10 yr. Each observation has a precision of 150 μas. For periods longer than 10 years, the curve shows the worst-case phase.

measuring periods that exceed the duration of the observing program. A search for Jupiter-mass planets around solar-type stars should have a duration of at least $\sim$10 yr to avoid this penalty. On the other hand, a nearby low-mass star with a large signal could be significantly detected even if it were in a much longer period orbit. For example, a Jupiter-mass planet in an 80 yr orbit around Barnard's star could be detected at 3 σ confidence in a 10 yr program because the expected signal is $\sim$58 mas.

6.3. *DCR Calibration*

In a search for planetary systems, the major systematic error will be DCR. Our experiment at the 5 m attained an accuracy of 0.59 mas at tan $(z) = 1$, compared to the predicted accuracy of 0.43 mas. Even if we were to limit observations to near the meridian and add declination constraints, e.g., within 1 hr of meridian crossing and at declinations within 45° of the zenith, the DCR calibration error using the three-filter calibration method would still be 128 μas. This is inadequate for a planetary search program that requires random errors of 100 μas per source per year (see below). An improvement is to use low-resolution spectroscopy. A time-effective method is to place a grating or grism in front of the CCD to perform slitless spectroscopy. Comparing $R_{\rm eff}$ of the spectra of Jacoby, Hunter, & Christian (1984) to $R_{\rm eff}$ derived from spectra smoothed to 20 nm, the residuals range from -220 μas for a B4 star to 102 μas for an M5 star. Assuming a worse case of 220 μas error in $R_{\rm eff}$, the DCR calibration error is only 66 μas when the observations are limited to declinations within 45° of zenith and ± 1 hr of meridian crossing. Thus we adopt $\sigma_{\rm DCR} = 66$ μas as a conservative estimate of the DCR error in the planetary search program.

6.4. *Geometric Calibration of the CCD*

Astrometric data analysis on CCDs has been discussed by Monet & Dahn (1983). We determine relative centroid positions of stellar images on the chip to perform relative astrometry. For example, to achieve an astrometric precision of 100 μas requires a centroid accuracy of 0.0016 pixel in our 5 m observations. This requirement is eased by the fact that the stellar images are spread over many pixels, e.g., 1″ images cover $\sim$200 pixels. Thus, assuming uncorrelated errors in relative pixel positions, the required centroid accuracy for each pixel is $0.0016 \times \sqrt{200} = 0.023$, well within current capabilities (Monet et al. 1992).

Systematic errors in pixel locations due to, for example, step and repeat errors in the CCD fabrication also introduce errors into the astrometric analysis. Shaklan & Pravdo (1994) discuss a method to calibrate such systematic errors. Shaklan & Pravdo (1994) and Shaklan et al. (1995) have demonstrated calibration accuracies in excess of this. Buffington et al. (1990) have shown that CCD photometric and dimensional stabilities are more than adequate for this experiment. Thus, $\sigma_{\rm CCD}$ is negligible.

We have explored the question of the long-term stability of CCD centroid measurements with regards to the stability of the electronics. We know from laboratory measurements that the charge-transfer efficiency, an important contributor to relative centroid determination, is not sensitive to the voltages of the clocking electronics within a broad operating range (Janesick 1993). We conclude that as long as the voltages are maintained within that range, then relative centroid motion is negligible.

6.5. *Optical Aberrations*

Astrometric accuracy can be limited by optical aberrations, especially distortion (Gatewood 1992). For large apertures and small fields of view, aberrations are small. As an example, we consider aberrations associated with the Keck 10 m telescope. Figure 6 shows the as-designed distortion for the Keck 10 m across an 84″ field of view (see § 7.1). The telescope has low intrinsic distortion and also low sensitivity to motion of the secondary mirror. These effects are negligible compared to other sources of error.

Another issue for the Keck 10 m is the effect of the primary segments on astrometry. Astrometric performance is insensitive to aberrations on the primary, since all stars are affected in the same way. The Keck segments are actively aligned to 50 mas rms. For 36 segments, this implies that centroid motion due to one segment will be 1400 μas, resulting in a average motion of 233 μas when the contributions per segment are random and independent. Therefore, to achieve astrometric accuracy at the $\sim$100 μas level, we require that *differential* effects due to segment misalignments be no more than $\sim$25% of the overall centroid motion. This is expected to be the case, since segment misalignments are well within the seeing disk diameter. Differ-

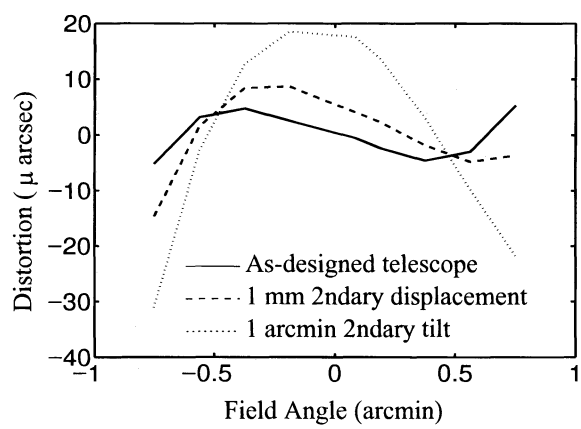

FIG. 6.—Distortion at the Keck telescope is well below the precision of the astrometric measurements. The solid curve is the as-designed distortion across an 84″ field of view. The other curves show how the distortion changes when the secondary mirror is misaligned.

© American Astronomical Society • Provided by the NASA Astrophysics Data System

1996ApJ...465..264P

ences in segment reflectivities over time may add another 10% to the effect of misalignments. Thus, σ_{ab} is also negligible.

7. IMPLICATIONS FROM THE PALOMAR RESULTS

7.1. *Aperture Dependence*

We use our 5 m results to extrapolate the ability to detect extrasolar planets with three apertures: 1.5, 5, and 10 m. For specificity, we use the optical parameters of the Palomar 1.5 m and the Keck 10 m. Table 3 lists the relevant parameters for the comparison. Most of the discussion will relate to the 10 m telescope, since it has by far the most potential.

The position of a target star is measured relative to a surrounding field of reference stars which form a fixed frame of reference. This technique was described by Eichhorn & Williams (1963) and is employed by Gatewood (1987). The reference stars allow us to make an affine transformation between observations (e.g., Shaklan et al. 1994). At least three reference stars are required to generate a linear model of the field; six reference stars are required for a quadratic model. Since we solve also for the parallaxes and proper motions, an additional reference star is required, resulting in a minimum of seven for the quadratic model. In any case, with more reference stars, the field model is more robust. It also accounts for optical aberrations (§ 6.5). If we consider a large-format CCD (e.g., 2048 × 2048 with 30 μm pixels), the field of view at the Keck telescope is 84″. This provides (Table 3) an average of 8.6 reference stars with $V \leq 21$ at $b^{II} = 30°$ (Allen 1973). A limiting magnitude of $V = 21$ is required because fainter stars do not provide enough photons. For purposes of comparison between the 10, 5, and 1.5 m telescopes, we choose fields of view that have the same average number of reference stars.

The reference frame has an effective brightness which depends on the intensity and spatial distribution of the stars. Monte Carlo simulations of reference fields show that the effective brightness is 5 times fainter than the summed light of the frame (see Appendix B). For the 10 m telescope, this translates into an effective reference frame magnitude of V = 19. The reference frame is effectively $V = 17$ at the 5 m telescope and $V = 16$ at the 1.5 m. In the analysis discussed below, the reference frame photometric centroid noise, σ_p, is computed by fitting a Gaussian profile to a star with magnitude equal to the effective reference frame magnitude. The Gaussian was fitted with a weighted least-squares algorithm, where the weight of each pixel in the sum of the squared residuals is given by the summed variances of photon noise, detector noise, and sky background. The algorithm is discussed in detail by Stone (1989). For the 10 m, 5m, and 1.5 m, $\sigma_p = 41$, 71, and 120 μas hr$^{1/2}$, respectively.

In all three cases, the atmospheric noise is substantially worse than the photometric noise and is the limiting factor for astrometric accuracy. The atmospheric noise was calculated using a Monte Carlo simulation of equation (7) for the parameters in Table 3. For the 10 m, 5m, and 1.5m, $\sigma_a = 87$, 240, and 850 μas hr$^{1/2}$, respectively.

TABLE 3

TELESCOPE COMPARISONS

PARAMETER	TELESCOPE 1.5 m	5 m	10 m
A. Specifications			
Image scale (30 μm pixel^{-1})	0″.476	0″.078	0.042
Field-of-view diameter	178″	133″	84″
Faintest reference star V	18	19	21
Number of reference stars ($b^{II} = 30°$)	8.6	8.6	8.6
Effective reference frame V	16	17	19
Sky (bright sky mag arcsec^{-2})	19	19	20
Brightest target star V	3.2	4.5	4.5
Seeing FWHM	1.0	1.0	0.5
B. "Solar Class" Search Results			
Stars searched (total)	50	100	100
F	0	0	13
G	0	9	39
K	8	29	48
M	42	62	0
Minimal outer AU searched	3.1	3.9	4.7

7.2. *Target Stars*

As shown in equation (8), the astrometric signal depends inversely on the distance to the star. Thus, nearby stars are the best candidates to search for planets using this method. The source catalog for stars within ~25 pc of the Sun is the *Preliminary Version of the Third Catalogue of Nearby Stars* or CNS3 (Gliese & Jahreiss 1993). CNS3 contains 3802 stars including three B, 73 A, 264 F, 486 G, 772 K, and 1097 M stars, We also treat 639 stars with color class "m" as M stars based upon their colors and absolute luminosities. We have verified spectroscopically that a number of these stars are M stars (Pravdo et al. 1995b). Stellar distances are inferred from the given trigonometric parallaxes or in some cases photometric and spectroscopic parallaxes. Stellar masses are determined using the relation

$$\log\left(\frac{M_S}{M_\odot}\right) = 0.118(4.75 - M_{\rm bol}) , \qquad (12)$$

with the stellar bolometric magnitude, $M_{\rm bol}$, taken from the spectral type, luminosity class, and bolometric corrections (Allen 1973). A minimum mass of 0.1 $M_\odot$ is assumed. For stars for which the luminosity class or subtype is not given, we assume luminosity class V and subtype 5. Stars with color types of "m" are assumed to be M5 dwarfs for the mass estimates. This is consistent with their absolute luminosities.

This sample is restricted in the following ways. First, to limit the effects of DCR (§ 3.2) we use a ±45° swath in declination around the zenith of the ground-based observatory site, Second, to ensure enough reference stars in each field (§ 7.1), we limit the galactic latitude of the target stars to $b^{II} \leq 30°$. Finally, we introduce a telescope- and detector-dependent V magnitude lower limit (Table 3) to prevent image saturation assuming a fast-readout region. This results in 838 candidates, consisting of two A, 25 F, 105 G, 174 K, 330 M, and 202 m stars, each of which has $\Theta \geq 300$ μas for a Jupiter-mass planet in a 10 yr orbit. Figure 7 shows the astrometric signals for these stars plotted in order of spectral type and subtype, with each subtype sorted by astrometric signal magnitude.

We keep some known binaries in the list of stars. Only those with small apparent separations are removed. Some short-period binaries will be discovered and eliminated early in an observational program. Long-period binaries both known and discovered are not expected to be different

© American Astronomical Society • Provided by the NASA Astrophysics Data System

1996ApJ...465..264P

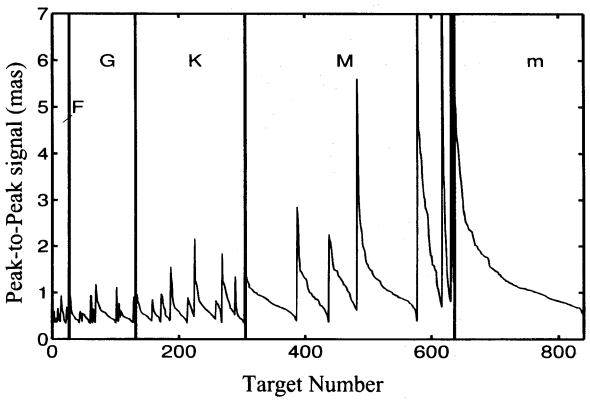

FIG. 7.—Peak-to-peak amplitudes of stellar motion for the 838 stars potentially sampled in a 10 m survey assuming the presence of a Jupiter-mass planet in a 10 yr orbit. Stars are sorted by spectral type and subtype, with each subtype sorted by amplitude. The y-axis of the plot cuts off Barnard's star, an M5 dwarf, that would have a 14.5 mas amplitude.

from single stars in the properties of their planetary systems. In studies of a subset of CNS3, less than 3% of the stars were in long-period binary systems (Wasserman & Weinberg 1991).

7.3. *Model Results*

An astrometric planet search program requires a significant and long-term allocation of telescope time: we assume a minimum of 40 nights per year. Since the survey is time and not source limited, the number of stars surveyed increases almost linearly with available observing time. We assume a bright sky for this analysis (Table 3). The observing efficiency due to bad weather and other effects is chosen to be 50%, resulting in a net observing time of 160 hr yr^{-1}. The observations should last for 10–20 yr to encompass the range of orbital periods in the search. Twice-yearly target star observations would result in a lower limit to the period search of $T = 1$ yr. DCR calibration observations are required but once and do not represent a significant amount of overhead.

The observation time per target determines the statistical significance of any detection as well as the range in parameter space over which that significance is valid. Since the planet periods are unknown, each target should be observed long enough so that an important range in that parameter space is sampled. We have chosen semimajor axis parameter space to display the results because it may be the parameter with the most physical interest. If, as suggested by Boss (1995), the radius at which gas giants form is 4-5 A.U. independent of stellar temperature or mass for masses as low as 0.1 $M_\odot$, then it will be crucial for any observing program, regardless of the stellar sample, to explore this area of parameter space. It is, of course, related directly to orbital period parameter space.

We examine two potiential surveys: each searches a statistically significant number of stars (≥ 100), but the first emphasizes "solar class" spectral types, with an average mass of 0.82 $M_\odot$, while the second emphasizes star numbers and contains mostly M-type stars. Figure 8 shows the detectable (3 σ) semimajor axes (shaded regions) for the solar class stars observed with the 10, 5, and 1.5 m telescopes in a 10 yr program. The number of stars is limited to 100 because the solar class spectral types are more massive and have lower signals, and thus each take more observing

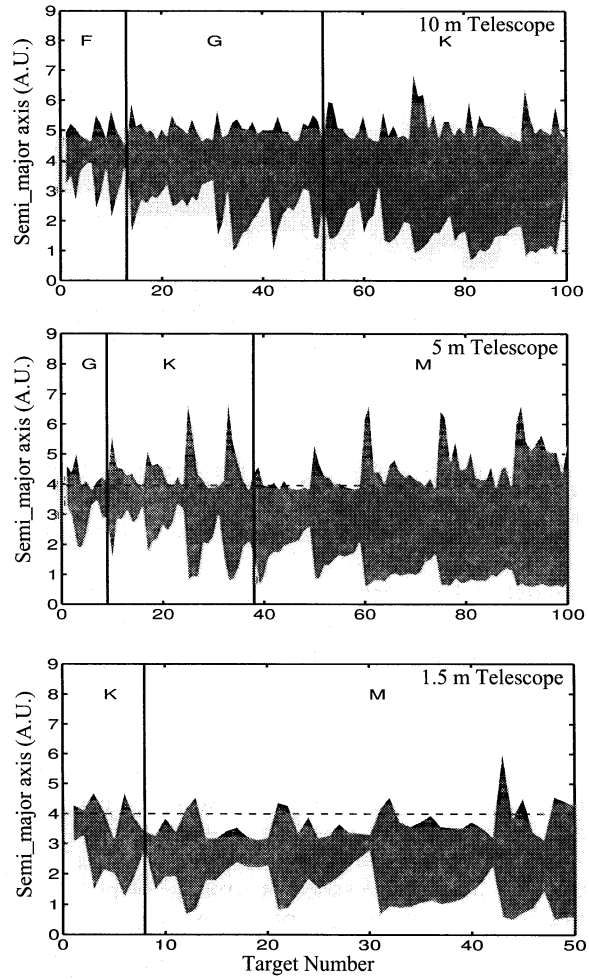

FIG. 8.—Parameter spaces explored (*shaded regions*) for 3 σ detection in a 10 yr program at the 10, 5, and 1.5 m telescopes. 160 hr yr^{-1} of observation time are divided equally among the sources. The Keck telescope explores the 4–5 A.U. region for nearly all the 100 program stars. A dashed line indicates the 4 A.U. boundary. The jagged edges of the shaded regions are due to varying distances and masses of the target stars.

time than M stars. For this survey $\sigma_o = 100$ μas, which is calculated from equation (11) with $\sigma_a = 87$ μas $hr^{1/2}$, $\sigma_p = 41$ μas $hr^{1/2}$, $\sigma_{DCR} = 66$ μas, $t = 1.6$ hr, and the other quantities negligible. We assume a 2000 Å bandpass and a 0.35 system throughput.

The target stellar types distribution is listed in Table 3. The figure and table demonstrate the utility of a larger aperture: in equal programs the 10 m observes more solar-like stars, 31 G stars compared to nine for the 5 m and zero for the 1.5 m, and it covers a larger area of semimajor axis parameter space for each star. Figure 9 shows the coverage gain in semimajor axis space with time, if the survey is extended beyond 10 years. After 20 years with the 10 m telescope, the space is searched to 10 A.U. for nearly the entire sample.

The second survey emphasizes the number of stars observed rather than a distribution of spectral types. In this case, the 10 m telescope can observe 574 stars, mostly of type M. With either survey, if there are no detections one could conclude that Jupiter-mass planets are uncommon in the samples.

Finally, one could search for lower mass planets with a more limited sample and reduced parameter space coverage. For example, a 10 m, 40 nights per year, 10 yr survey

© American Astronomical Society • Provided by the NASA Astrophysics Data System

1996ApJ...465..264P

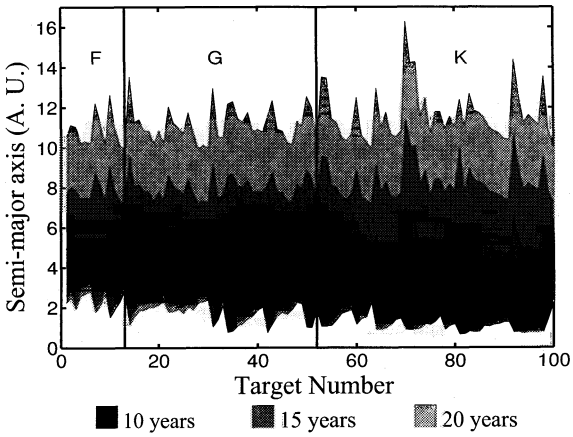

FIG. 9.—The semimajor axis parameter space searched with a 10 m telescope expands as the observational program length increases. The 10 yr search region is identical to that in Fig. 8.

could detect 43 Saturn-mass planets around two G, eight K, and 33 M stars, or five Uranus-mass planets around M stars. For the latter survey, the maximum semimajor axes are only 3.2 A.U.

8. CONCLUSIONS

We have used the Palomar 5 m telescope to achieve astrometric precisions of 0.1 mas over periods of minutes in a 90″ field of view. The observations are not limited by systematic errors. We apply our observational results to show that a large telescope is capable of performing statistically significant surveys of nearby stars for Jupiter-mass planets. While any such program requires careful, continuing long-term calibration, it does not place extraordinary requirements on any one of the random sources of astrometric noise. The final error per observation, 100 μas, would be a factor of 10 better than that currently obtained with smaller apertures.

The number of surveyed stars should be ≥ 100 because one expects to detect several Jupiter-mass planets in so large a sample if the canonical model of solar system formation is correct. Systems with detected Jupiter-mass planets would be prime targets for terrestrial planet searches. If no Jupiter-mass planets are found in a sample of 100 "solar-like" stars, one would conclude that there is only a 3×10^{-5} probability that gas giant planets as large or larger than Jupiter form in at least 10% of the systems. This conclusion would be approximate, since the same areas of semimajor axis parameter space are not searched for each star.

If a survey of mostly M stars is performed, one must assume that Jupiter-mass planets can contain up to 0.01 of the system mass, or an amount 10 times higher than in the solar system. Boss (1995) concludes that such systems could exist and that the gas giant planets could be located at 4–6 A.U. separations from their stars.

In searches for planetary systems similar to ones described above, gas giant planets can be detected. Furthermore, the absence of detectable Jupiter-mass planets would begin to put pressure on the theory that planetary systems like the solar system are common.

We acknowledge Mark Colavita, George Gatewood, Anthony Gleckler, Hiroshi Kadogawa, Eugene Levy, David Monet, and Michael Shao for useful discussions. We also thank the anonymous referee for suggesting significant improvements to an earlier version.

APPENDIX A

Lindegren (1980) derived an equation for the variance due to atmospheric turbulence of the measurement of a target star relative to a field of background stars. He defined the position of the target star as ϕ_0 and the positions of the reference stars as ϕ_i where $i = 1, 2, \ldots, n$ for n reference stars. The variance was then defined as

$$\epsilon^2 = \left\langle \left(\phi_0 - \frac{1}{n} \sum_{i=1}^{n} \phi_i \right)^2 \right\rangle . \tag{A1}$$

Lindegren then estimated the field averaging effect by assuming that the variance between any two stars ϕ_i and ϕ_j was only a function of their separation θ_{ij}, so that $\langle (\phi_i - \phi_j)^2 \rangle = f(\theta_{ij})$. For f, he invoked the differential image motion equation (his eq. [18a]),

$$f(\theta) = 2K_\alpha C k^{-2} [\alpha(\alpha + 1) D^{\alpha - 3} (\theta h)^2 - 2D^{-2} (\theta h)^{\alpha + 1}] (vt)^{-1} , \tag{A2}$$

where $\alpha = 5/3$ for a Kolmogorov turbulence spectrum, and other parameters were derived by assuming a Hufnagel (1974) structure profile, seeing parameter $r_0 = 0.1$ m, and a wind speed profile from Gringorten et al. (1965). Other parameters in the equation are D = aperture diameter in meters and t = integration time in seconds; θ is expressed in radians.

Then he considered the continuous limit, where $n \to \infty$ and the target star is centered in the field. Equation (A2) then reduces to his equation (36a), valid for long integrations and narrow fields of radius R radians,

$$\epsilon^2 \simeq 9.3 \times 10^6 D^{-2} R^{8/3} t^{-1} . \tag{A3}$$

The first term (proportional to θ^2) of equation (A2) drops out in the continuous and symmetric limits. This term, however, is important for any real case in which the target star is at the center of the field.

From Lindegren's results, it is possible to derive an expression valid for any distribution of reference stars. By combining equations (A2) and (A3) with Lindegren's equation (26a), one can evalute equation (A2) to obtain

$$f(\theta) = 2.9 \times 10^5 (D^{-4/3} \theta^2 - 192 D^{-2} \theta^{8/3})^{t-1} . \tag{A4}$$

© American Astronomical Society • Provided by the NASA Astrophysics Data System

1996ApJ...465..264P

Equation (A1) can then be reevaluated to obtain

$$\epsilon^2 = n^{-2}t^{-1}\sum_{i=1}^{n}\sum_{j=1}^{n}\left[f(\theta_{0i}) - \frac{1}{2}f(\theta_{ij})\right] = \frac{2.9\times 10^5}{n^2 t}\left[\sum_{i=1}^{n}\sum_{j=1}^{n}D^{-4/3}\left(\theta_{0i}^2 - \frac{1}{2}\theta_{ij}^2\right) - 192\sum_{i=1}^{n}\sum_{j=1}^{n}D^{-2}\left(\theta_{0i}^{8/3} - \frac{1}{2}\theta_{ij}^{8/3}\right)\right]. \quad \text{(A5)}$$

One can show that the sum over the θ^2 terms is proportional to the squared distance between the target star and the field centroid; hence, it does not appear in Lindegren's continuous symmetric limit. When the target star is near the centroid of the reference stars, the first term ($\propto \theta^2$) of equation (A5) is small compared to the second term ($\propto \theta^{8/3}$). The second term of equation (A4) then limits the astrometric precision.

Lindegren's results do not account for the direction (e.g., R.A. or decl.) of the variance. Shao & Colavita (1992) in their appendix showed that independent of turbulence direction, the only nonzero noise contributions in long exposures are parallel to the stellar separation. Therefore, one can predict the R.A. and declination noise from a given field of reference stars by replacing θ_{ij} in equation (A5) with the angular separations δ_{ij} projected onto the respective axes. The final result is

$$\epsilon^2 = \frac{2.9\times 10^5}{n^2 t}\left[\sum_{i=1}^{n}\sum_{j=1}^{n}D^{-4/3}\left(\delta_{0i}^2 - \frac{1}{2}\delta_{ij}^2\right) - 192\sum_{i=1}^{n}\sum_{j=1}^{n}D^{-2}\left(\delta_{0i}^{8/3} - \frac{1}{2}\delta_{ij}^{8/3}\right)\right]. \quad \text{(A6)}$$

APPENDIX B

The target star position is measured relative to the reference frame formed by the background stars. Observations made at different epochs are registered to one another using an affine transformation that is defined with a least-squares model. Simple models (e.g., linear in each axis) require fewer reference stars and are less sensitive to random noise in their parameter variance than higher order models. Higher order models, on the other hand, are sometimes required to account for aberrations and other systematic effects. In this appendix, we show how the reference star distribution and choice of affine transformation relate to the astrometric sensitivity of the model.

Since the target stars are generally brighter than the background stars, astrometric precision is limited by the photometric noise associated with the background stars. In this Appendix, we compute the noise in the estimate of the target star position as a function of the reference frame spatial and brightness distribution, for both linear and second-order models.

The affine transformation is defined by a set of parameters, β, that provide a least-squares solution to the equation

$$W^{-1}Y = W^{-1}X\beta\,. \quad \text{(B1)}$$

Y is the vector of measured background star positions in frame i, which for the x axis positions is given by

$$Y = \begin{bmatrix} x_{i,1} \\ x_{i,2} \\ \vdots \\ x_{i,n} \end{bmatrix}, \quad \text{(B2)}$$

where the second subscript refers to star number, and there are n background stars. X defines the affine transformation in terms of measured positions in frame $j \neq i$. For three linear terms per axis, X is given by

$$X = \begin{bmatrix} 1 & x_{j,1} & y_{j,1} \\ 1 & x_{j,2} & y_{j,2} \\ & \vdots & \\ 1 & x_{j,n} & y_{j,n} \end{bmatrix}. \quad \text{(B3)}$$

W^{-1} gives the weight of each equation. When the measurement error of each star is independent with a standard deviation σ_m, $m = 1, \ldots, n$, then W takes the form

$$W = \begin{bmatrix} \sigma_1 & & & \\ & \cdot & 0 & \\ & & \cdot & \\ & 0 & \cdot & \\ & & & \sigma_n \end{bmatrix}. \quad \text{(B4)}$$

The noise will be independent when, as considered below, the noise is due to the photon statistics of each star.

The solution to equation (B1) is given by (see, e.g., Press et al. 1989)

$$\hat{\beta} = (X^T V^{-1} X)^{-1} X^T V^{-1} Y\,, \quad \text{(B5)}$$

with $V = W^T W$, the diagonal matrix of positional variances. The covariance matrix of the solution is given by

$$\mathrm{cov}\,(\hat{\beta}) = (X^T V^{-1} X)^{-1}\,. \quad \text{(B6)}$$

We assume now that the target star is located nominally at the center of the coordinate frame. The variance of the positional error of the center of the frame is given by the first term in the covariance matrix, $\sigma_f^2 = \mathrm{cov}\,(\hat{\beta})(1, 1)$. For the linear

© American Astronomical Society • Provided by the NASA Astrophysics Data System

1996ApJ...465..264P

model of equation (B3), this term is

$$\sigma_f^2 = \left(\Sigma \frac{x_m^2}{\sigma_m^2} \Sigma \frac{y_m^2}{\sigma_m^2} - \Sigma \frac{x_m y_m}{\sigma_m^2}\right)\left[\Sigma \frac{1}{\sigma_m^2} \Sigma \frac{x_m^2}{\sigma_m^2} \Sigma \frac{y_m^2}{\sigma_m^2} - \Sigma \frac{1}{\sigma_m^2} \Sigma \frac{x_m y_m}{\sigma_m^2} - \left(\Sigma \frac{x_m}{\sigma_m^2}\right)^2 \Sigma \frac{y_m^2}{\sigma_m^2} + 2\Sigma \frac{x_m}{\sigma_m^2} \Sigma \frac{y_m}{\sigma_m^2} \Sigma \frac{x_m y_m}{\sigma_m^2} - \left(\Sigma \frac{y_m}{\sigma_m^2}\right)^2 \Sigma \frac{x_m^2}{\sigma_m^2}\right]^{-1} . \tag{B7}$$

We can rewrite this equation in terms of the moments of the background star distribution and the number of photons in the reference frame. If all stars have the same point-spread function, with rms width σ_c, and if the centroid measurement noise on star m is due strictly to the finite number of detected photons, N_m, then the positional variance of star m is given by

$$\sigma_m^2 = \frac{\sigma_c^2}{N_m} . \tag{B8}$$

Substituting this into equation (B7), and defining the moments of the field as

$$M_{1x} = \frac{\Sigma N_m x_m}{\Sigma N_m} , \tag{B9}$$

$$M_{2x} = \frac{\Sigma N_m x_m^2}{\Sigma N_m} , \tag{B10}$$

$$M_{x,y} = \frac{\Sigma N_m x_m y_m}{\Sigma N_m} , \tag{B11}$$

and similarly for M_{1y} and M_{2y}, one then finds

$$\sigma_f^2 = \frac{\sigma_c^2}{\Sigma N_m} \cdot \frac{M_{2x} M_{2y} - (M_{xy})^2}{M_{2x} M_{2y} - (M_{xy})^2 - M_{1x}^2 M_{2y} + 2M_{1x} M_{1y} M_{xy} - M_{1y}^2 M_{2x}} . \tag{B12}$$

Equation (B12) shows that the target star positional variance is given by the width of the stellar images σ_c, the total light in the frame ΣN_m, and a function of the first and second moments of the reference frame.

If the plate scale model was not required, and if only one reference star of brightness ΣN_m was present, then the first term of equation (B12) would be the reference frame positional variance, given by σ_1^2. The second term containing the moments can be thought of as the inefficiency of the plate scale model. The positional variance for astrometry is then the product of the noise associated with a single reference star of brightness ΣN_m and a frame efficiency factor F given by the ratio of moments in equation (B12).

For higher order transformations, the number of terms in equation (B12) grows rapidly. Matrix inversion for a full quadratic model (six terms per axis) is made possible under the assumption that the field is point symmetric. In that case, the frame variance is given by

$$F = \frac{M_{4x} M_{4y} - [M_{2(xy)}^2]}{M_{4x} M_{4y} - [M_{2(xy)}^2] - M_{2x}^2 M_{4y} + 2M_{2x} M_{2y} M_{2(xy)} - M_{2y}^2 M_{4x}} . \tag{B13}$$

The presence of fourth-order moments implies that for quadratic models the frame variance is highly sensitive to the distribution of reference stars. Note that for the linear model, $F = 1$ when the field is assumed to be point symmetric.

An interesting characteristic of equation (B12) is that the variance depends on the shape but not the size of the field. This is shown easily by substituting $x' = ax$ into equations (B9) to (B11), a being a scale factor. This is in contrast to differential centroid noise due to the atmosphere, which is not considered in this Appendix. Atmospheric noise, in the small-field limit, increases linearly with field diameter.

The value of F depends on the distribution of reference stars. We have arrived at a mean value of F by performing a Monte Carlo simulation of reference frames. In the simulation, reference stars having $V \leq 21$ were chosen with a magnitude distribution taken from Allen (1973) and positioned randomly within the field of view of the 10 m telescope (84″; Table 3). Reference frames were required to have at least six stars and were defined over the whole sky. The moments were evaluated according to equations (B9)–(B11), and F was evaluated according to equation (B12). The result was that the mean value of F for the linear affine transformation was $F \approx 5$.

Thus, as reported in § 7.1, the reference frame, when reduced using a linear affine transformation, is effectively 5 times fainter than the summed light of the reference frame. The same fields reduced with a full quadratic model had an effective brightness 31 times fainter than the summed reference frame.

REFERENCES

Allan, D. W. 1966, Proc. IEEE, 54, 221
Allen, C. W. 1973, Astrophysical Quantities (London: Athlone Press)
Anthony-Twarog, B. J., et al. 1990, AJ, 99, 1504
Black, D. C., & Matthews, M. S. 1985, Protostars and Planets II (Tucson: Univ. Arizona Press)
Black, D. C., & Scargle, J. D. 1982, ApJ, 263, 854
Boss, A. P. 1995, Science, 267, 360
Boss, A. P., & Yorke, H. W. 1993, ApJ, 411, L99
Buffington, A., et. al. 1990, PASP, 102, 688
Burke, B. F., et al. 1993, TOPS: Toward Other Planetary Systems, Solar System Exploration Division Report (Washington, DC: NASA)
Cochran, W. D., Hatzes, A. P., & Hancock, T. J. 1991, ApJ, 380, L35

© American Astronomical Society • Provided by the NASA Astrophysics Data System

1996ApJ...465..264P

Colavita, M. M. 1994, A&A, 283, 1027
Dekany, R., et al. 1994, Ap&SS, 212, 299
Eichhorn, H. K., & Williams, C. A. 1963, AJ, 68, 221
Gatewood, G. 1987, AJ, 94, 213
———. 1991, BAAS, 23, 1433
———. 1992, in Astrometric Imaging Telescope 1991 Final Report, ed. S. Pravdo (JPL pub. D-9651), 85
Gil, J. A., et al. 1993, A&A, 271, L17
Gliese, W., & Jahreiss, H. 1993, Preliminary Version of the Third Catalogue of Nearby Stars (CNS,3), preprint
Gringorten, I. I., et al. 1965, Handbook of Geophysics and Space Environment, ed. S. L. Valley (New York: McGraw-Hill)
Hufnagel, R. E. 1974, Digest of Technical Papers, Topical Meeting on Optical Propagation through Turbulence (Washington, DC: Optical Society of America), Wa1
Jacoby, G. H., Hunter, D. A., & Christian, C. A. 1984, ApJS, 56, 257
Janesick, J. 1993, in Astrometric Imaging Telescope 1992 Final Report, ed. S. Pravdo (JPL Internal Document, JPL D-10760), 369
Latham, D. W., et al. 1989, Nature, 336, 38
Levy, E. H., et al. 1992, Protostars and Planets III (Tucson: Univ. Arizona Press)
Lindegren, L. 1980, A&A, 89, 41
Marcy, G. W., et al. 1993, Remote Sensing Rev., 8, 205
Marcy, G. W., & Butler, P. 1995, IAU Circ. No. 6251
Marsh, K. A., & Mahoney, M. J. 1992, ApJ, 395, L115
———. 1993, ApJ, 405, L71
Mayor, M., & Queloz, D. 1995, Nature, 378, 355
McCarthy, J. K. 1994, Proc. SPIE, 2198, 163
McMillan, R. S., et al. 1994, Ap&SS, 212, 271
Monet, D., et al. 1992, AJ, 103, 638
Monet, D., & Dahn, C. C. 1983, AJ, 88, 1489
Peale, S. J. 1993, AJ, 105, 1562
Pravdo, S. H. et al. 1995a, Nature, submitted
———. 1995b, in preparation
Press, W. H., et al. 1989, Numerical Recipes (Cambridge: Cambridge Univ. Press)
Safronov, V. S. 1969, Evolution of the Protoplanetary Cloud and Formation of the Earth and the Planets (Moscow: Nauka)
Safronov, V. S., & Ruskol, E. L. 1994, Ap&SS, 212, 13
Shaklan, S. & Pravdo, S. H. 1994, SPIE, 2198, 1227
Shaklan, S., et al. 1994, Ap&SS, 212, 453
———. 1995, Appl Opt., 34, 6672
Shao, M., & Colavita, M. M. 1992, A&A, 262, 353
Smith, B. A., & Terrile, R. J. 1984, Science, 226, 1421
Stone, R. C. 1989, AJ, 97, 1227
Stone, R. C., & Dahn, C. C. 1994, in IAU Symp. 166 Astronomical and Astrophysical Objectives of Sub-milliarcsecond Optical Astrometry, ed. E. Hog and P. K. Seidelmann (The Hague: Kluwer)
Wasserman, I., & Weinberg, M. D. 1991, ApJ, 382, 149
West, F. R. 1967, ApJS, 14, 384
Wolszan, A., & Frail, D. A. 1992, Nature, 355, 145

© American Astronomical Society • Provided by the NASA Astrophysics Data System